FATIGUE PERFORMANCE COMPARISON AND LIFE PREDICTION OF FORGED STEEL AND DUCTILE CAST IRON CRANKSHAFTS

JONATHAN WILLIAMS, FARZIN MONTAZERSADGH, AND ALI FATEMI
GRADUATE ASSISTANTS AND PROFESSOR, RESPECTIVELY
MECHANICAL, INDUSTRIAL & MANUFACTURING ENGINEERING DEPARTMENT
THE UNIVERSITY OF TOLEDO, TOLEDO, OHIO

ABSTRACT

The objective of this study was to compare the durability of crankshafts from two competing manufacturing processes, as well as to perform dynamic load and stress analysis, and optimization. The crankshafts used in the study were forged steel and ductile cast iron from a one-cylinder gasoline engine. Strain-controlled monotonic and fatigue tests as well as impact tests were performed on specimens machined from the crankshafts. Load-controlled component bending fatigue tests were also carried out on the crankshafts. Material tests showed that the forged steel had 26% higher tensile strength and 37% higher fatigue strength than the ductile cast iron, while component tests showed that the forged steel crankshaft had 32% higher fatigue strength resulting in a factor of six longer fatigue life. The S-N approach used to predict the fatigue lives of both crankshafts showed reasonable correlation to the experimental data from the component tests. Dynamic load analysis was performed to determine the in service loading of the crankshafts and FEA was conducted to find stresses at critical locations. Finally, the geometry, material, and manufacturing processes were optimized for the forged steel crankshaft. The optimization process included geometry changes compatible with the current engine, fillet rolling, and the use of MA steel, resulting in 18% weight reduction, increased fatigue strength and reduced cost of the crankshaft.

INTRODUCTION

A crankshaft is a highly stressed component in an engine that is subjected to bending and torsional loads. The crankshaft must be designed to last the life of the engine due to the catastrophic damage to the engine which would result if failure did occur. Considering the life of an engine in an automobile, for example, this results in requirement for an infinite life fatigue situation. Because of the long life and high stresses, as well as the need for weight reduction, material and manufacturing process selection is important in crankshaft design.

There is competition among materials and manufacturing processes, due to cost, performance, and weight. This is a direct result of industry demand for components that are lighter, to increase efficiency, and cheaper to produce, while at the same time maintaining fatigue strength and other functional requirements.

There are several ways to manufacture a crankshaft, including machining from a billet, forging, and casting. Due to cost and time, machining a crankshaft from a billet is seldom used except in very low production applications. The two most common types of crankshafts are made of cast iron and forged steel. One must also consider other design issues such as surface treatment techniques including induction hardening,

nitriding, and fillet rolling, and material selection such as microalloyed steels (1) and austempered ductile iron (ADI) (2), to name a few.

Many studies, including the one conducted by Jensen (3) on the V-8 automotive crankshaft, identify the critical location of the crankshaft as the fillet connecting the crank-pin to the web of the crankshaft. In order to increase the fatigue strength of crankshafts, the crank-pin fillets are often rolled in order to induce compressive residual stresses. The effects of residual stresses on crankshafts were analyzed and presented by Chien et al. (4).

A complete literature review on crankshafts was conducted and published by Zoroufi and Fatemi (5). In this literature review, the design aspects as well as manufacturing process steps for cast and forged crankshafts were presented and the effects of influential parameters such as residual stresses on fatigue behavior and methods of their production in crankshafts were discussed. The review also included a comparison of crankshaft material and manufacturing process technologies in terms of their durability performance, as well as assessment procedures used for crankshafts including bench testing and experimental techniques. Geometric optimization of crankshafts was also briefly discussed and cost analysis with potential cost savings from several studies in the literature were presented.

The objectives of this study were to compare the fatigue performance of ductile cast iron and forged steel crankshafts, perform a dynamic analysis and FEA to determine loading and stresses, respectively, as well as perform optimization on the forged steel crankshaft. The crankshafts used in the study were a 1045 forged steel crankshaft weighing 3.9 kg (8.6 lb) and a ductile cast iron crankshaft weighing 3.7 kg (8.2 lb). Both crankshafts were designed to be used in one-cylinder gasoline engines typical to those used in riding lawnmowers. The forged steel crankshaft was designed for a 460cc (28.1 in^3) engine generating 9.3 kW (12.5 HP), while the ductile cast iron crankshaft was from a similar size engine. The two crankshafts are shown in their finished, as tested, condition in Figure 1.

MATERIAL BEHAVIOR AND COMPARISONS

Experimental Program

Round specimens were machined from the cylindrical portions of the crankshafts which were in their unmachined, as forged and as cast states. Standard specimen geometry was used, with the exception of the grip section length, which was shortened slightly to maximize the number of specimens from each crankshaft (see Figure 2a). The specimens were polished after machining to remove all machining marks.

Testing was performed on a 50 kN (11 Kip) closed-loop servo-hydraulic uniaxial test frame controlled by a digital servo-controller. Strain was controlled by an extensometer that was rated as ASTM class B1. The load train consisting of the load cell, actuator, grips, and specimen, were carefully aligned prior to testing. Any misalignment from tilt or eccentricity in the load frame can result in bending strain in the specimens. ASTM Standard E606 (6) states that the maximum bending stress should not exceed 5% of the minimum axial strain range imposed during testing. An alignment bar fitted with strain gages along with an alignment fixture attached to the load frame

was used to make alignment. Testing was performed at room temperature which was monitored during the test along with the humidity. Monotonic and fatigue tests were performed according to ASTM Standard E8 (7) and ASTM Standard E606, respectively.

For the constant amplitude uniaxial fatigue tests, strain amplitudes ranging from 0.16% to 2% were used for the forged steel and 0.135% to 2% for the ductile cast iron. All tests were conducted in strain control, with the exception of some long life tests which were switched to load control after the load had stabilized in strain control. For strain-controlled tests frequencies ranged from 0.1 Hz to 1 Hz depending on the strain amplitude and remained the same if the test was switched from strain control to load control. If the strain was all elastic in strain control, the frequency was increased to 25 Hz when the test was switched to load control in order to minimize the time required for each test. Triangular waveform was used for each test with the data being recorded every 2^n cycles.

In order to compare the impact toughness of the two materials, Charpy V-notch tests were also performed. Impact toughness is relevant to crankshafts in applications such as for the case of lawnmower engines, where a sudden stop could result in an impact type loading condition in the engine. The standard 10 mm x 10 mm x 55 mm (Type A) specimen geometry was machined from the two components. For the forged steel, two directions were used, L-T and T-L. The specimen orientation is shown in Figure 2(b). For the L-T specimens, the specimen was oriented such that the longitudinal axis of the crankshaft was normal to the crack plane and the transverse direction was the direction of crack growth. The T-L specimens had the opposite orientation. In the forging process inclusion become elongated in the direction of maximum grain flow, thus causing the material properties to depend on the orientation. Only one direction was used for the cast crankshafts, since the inclusions and porosity are randomly oriented. The L-T specimens were removed from the main journal section of the forged steel crankshaft, while the T-L specimens were machined from the web section. The cast specimens were also removed from the web section.

Testing was performed on a pendulum type impact testing machine as outlined by ASTM Standard E23 (8). Tests were conducted at six temperature levels. Different conditioning methods were used including dry ice and isopropanol alcohol, ice bath, ambient, or electric oven, depending on the temperature. Two specimens were tested for each material/orientation for each temperature level.

Experimental Results and Comparisons

The monotonic and cyclic properties for the two materials are summarized in Table 1. The results show that the yield strength of the ductile cast iron is 66% of the yield strength for forged steel, while the ultimate strength for the ductile cast iron is 80% of that of forged steel. As a comparison of the ductility of the materials the percent reduction in area (%RA) for the forged steel was 58% while the ductile cast iron was only 6%, which shows that even though the cast iron is ductile iron, forged steel has much more ductility.

Superimposed plots of the cyclic and monotonic stress-strain curves for the two materials are shown in Figure 3. The monotonic curve is represented by the following equation:

$$\varepsilon = \frac{\sigma}{E} + \left(\frac{\sigma}{K}\right)^{1/n} \qquad (1)$$

For the cyclic curve, equation (1) is also used, with the stress and strain terms replaced by their amplitudes and K and n replaced by K' and n'. Values of K, n, K', and n' are listed in Table 1. The figure shows that the ductile cast iron material exhibits a strain hardening behavior, as indicated by the cyclic curve being above the monotonic curve. The forged steel material showed a slight cyclic softening behavior, indicated by the cyclic curve being below the monotonic curve.

The stress-life (S-N) behavior of the material is described by the equation:

$$\frac{\Delta\sigma}{2} = \sigma_f' \left(2N_f\right)^b \tag{2}$$

Equation (2) was used to determine the fatigue strength at 10^6 cycles for the two materials. Steels can exhibit a fatigue limit at 10^6 cycles, below which failure does not typically occur. It has been shown that the S-N curve for cast irons continues to decline past 10^6 cycles and the fatigue limit, if any, occurs at greater than 10^6 cycles. The fatigue strength at 10^6 cycles for forged steel was determined to be 359 MPa (52.1 ksi) and for the cast iron to be 263 MPa (38.1 ksi). Therefore the fatigue strength at 10^6 cycles was 37% higher for forged steel than the cast iron. This results in a factor of 30 longer life for the forged steel than the cast iron in the high cycle region. The true stress amplitude versus reversals to failure is shown in Figure 4(a).

Typically in automotive crankshaft design, the true plastic strain versus reversals to failure would serve little purpose since the loading would be all elastic due to the very large number of cycles (Giga cycles). However, in this particular application being for a lawnmower engine, it is possible that the crankshaft be subjected to impact loading conditions, such as a sudden stop if the blade makes contact with a hard object, subjecting the crankshaft to plastic strain at stress concentrations. The true plastic strain plot is shown in Figure 4(b), which indicates that the forged steel has more than an order of magnitude longer life than the cast iron for a given plastic strain amplitude. The equation of the plastic line is represented by:

$$\frac{\Delta\varepsilon p}{2} = \varepsilon_f' \left(2N_f\right)^c \tag{3}$$

Total strain amplitude is obtained by adding the elastic and plastic strain amplitudes, represented by the following equation:

$$\frac{\Delta\varepsilon}{2} = \varepsilon_a = \frac{\sigma_f'}{E}\left(2N_f\right)^b + \varepsilon_f' \left(2N_f\right)^c \tag{4}$$

The strain-life curves for both materials are shown in Figure 4(c), which shows that for a given strain amplitude, the forged steel has longer life than the cast iron by about an order of magnitude at long lives.

Fatigue behavior at notches is typically controlled by both stress and strain at the root of the notch. Therefore, the Neuber parameter which combines both stress and strain amplitudes can better represent fatigue behavior at notches, such as the fillets in a crankshaft. The Neuber parameter represented by the following equation:

$$\sqrt{(\Delta\sigma)(\Delta\varepsilon)E} = 2\sqrt{\left(\sigma_f'\right)^2\left(2N_f\right)^{2b} + \sigma_f'\varepsilon_f' E\left(2N_f\right)^{b+c}} \tag{5}$$

The Neuber curve shown in Figure 4(d) shows that for a given Neuber stress range the forged steel has a longer life than the cast iron by approximately a factor of 50. Note that values of the constants used in equations (1) through (4) for the two materials are given in Table 1.

The average results from the two Charpy V-notch specimens at each temperature are presented graphically in Figure 5. The figure shows that the forged steel in the L-T direction had the highest impact toughness regardless of temperature followed by the T-L direction. Both orientations of the forged steel had significantly higher impact toughness than the cast iron for all temperatures considered. More details of the monotonic, fatigue, and impact test procedures and results are provided by Williams and Fatemi in (9).

DYNAMIC LOAD ANALYSIS

Schematic of the digitized forged steel crankshaft investigated in this study is shown in Figure 6. The single cylinder engine configuration is shown in Table 2 and piston pressure versus crankshaft angle is shown in Figure 7. There are two different load sources acting on the crankshaft. Inertia of rotating components (e.g. connecting rod) applies forces to the crankshaft and this force increases with the increase of engine speed. The second load source is the force applied to the crankshaft due to gas combustion in the cylinder which is considered to be constant for different engine speeds (10).

Considering a slider-crank mechanism for the dynamic analysis the angular velocity and angular acceleration of the connecting rod and forces between the crankshaft and the connecting rod could be calculated using ADAMS, which is a dynamic analysis software program. Forces applied to the crankshaft cause bending and torsion. Figure 6 demonstrates the positive directions and local axis on the contact surface with the connecting rod.

Figure 8 shows the variations of bending and torsion loads and the magnitude of the total force applied to the crankshaft as a function of crankshaft angle during an engine cycle for the engine speed of 3600 rpm. The maximum load which happens at 355 degrees is where combustion takes place. At this moment the acting force on the crankshaft is just bending load since the direction of the force is exactly toward the center of the crank radius (i.e. $F_y = 0$ in Figure 6).

Figure 9 compares the magnitude of maximum torsional and bending loads at different engine speeds. As can be seen in this figure, the maximum of total load magnitude, which is equal to the maximum of bending load, decreases as the engine speed increases. The reason for this situation refers to the load sources that exist in the engine at 355 degree crank angle. At this crank angle these two forces act in opposite directions. The force caused by combustion which is greater than the inertia load does not change at different engine speeds since the same pressure versus crankshaft angle is used for all engine speeds. The load caused by inertia, however, increases in magnitude as the engine speed increases. Therefore, as the engine speed increases, the total load magnitude decreases. As a result, the minimum operating speed of 2000 rpm was considered as the critical loading condition. This speed is the minimum operating speed for this specific engine.

FINITE ELEMENT ANALYSIS

Modeling

FEA for dynamic loading was done by superposition of static loading cases. The main idea of superposition is finding the basic loading positions, then applying unit load on each position according to dynamic loading of the crankshaft, and scaling and combining the stresses from each unit load. The main advantage of dynamic analysis is more accurate estimation of the maximum and minimum loads. Design and analysis of the crankshaft based on static loading can lead to very conservative results.

The FE model of the crankshaft geometry has about 10^5 quadratic tetrahedral elements, with the global element length of 5.08 mm and local element length of 0.762 mm at the fillets where the stresses are higher due to stress concentrations. The meshed forged steel crankshaft with 122,441 elements is shown in Figure 10.

Boundary conditions in the FE model were based on the engine configuration. The mounting of the crankshaft considered is on two different bearings which results in different constraints in the boundary conditions. One side of the crankshaft is fixed to the engine block by a ball bearing and the other side is rolling over a journal bearing, as shown in Figure 11(a). When under load, only 180 degrees of the bearing surfaces facing the load direction constraint the motion of the crankshaft. These defined boundary conditions are shown in Figure 11(b). Boundary conditions rotate with the direction of the load applied such that the semicircular fixed surface and the ring in Figure 11(b) face the direction of the load.

It should be noted that although the FE modeling shown in this section is for the forged steel crankshaft, similar analysis was also performed for the ductile cast iron crankshaft.

Results and Discussion

Some locations on the geometry were considered for depicting the stress history. These locations were selected according to the results of FE analysis, and as expected, all the selected elements are located on different parts of the fillet areas due to the high stress concentrations at these locations. Selected locations are labeled in Figure 12(a) and the von Mises stresses with sign for these elements are plotted in Figure 12(b). The critical loading situation is when the speed engine is 2000 rpm and at the crank angle of 355 where the combustion exerts a large impact on the piston. At this time all stresses are at their highest level during stress time history in a cycle. As can be seen, location number 2 experiences the highest stress at this moment. Therefore, element number 2 was selected as the critical element.

Figure 12(c) shows the von Mises stress contour for the forged steel crankshaft. Figure 12(d) shows the maximum stress, mean stress, and stress range at the engine speed of 2000 rpm at different locations. It can be seen that element number 2 not only has the maximum von Mises stress, but it also carries the largest stress range and mean stress among other locations. This is important in fatigue analysis since the range and mean stresses have more influence than the maximum stress. This is another reason for why having the stress history of critical elements are more useful than static analysis of the crankshaft. Figure 13 shows variation of von Mises stress at location 2 for different engine speeds for the crankshaft. As can be seen in this figure, with the increase of engine speed the maximum stress and therefore stress range decreases. Therefore, the critical engine speed will be the lowest operating engine

speed which is 2000 rpm according to the engine manual. However, it should be noted that at high engine speeds other factors such as wear and lubrication become very important. As these issues were not of concern in this study, further discussion is avoided.

The von Mises stress at location number 2 shown in Figure 12(a) remains the same with and without considering torsional load. This is due to the location of the critical point which is not influenced by torsion since it is located on the crankpin bearing. Therefore, torsional load has no effect on the stress range of the critical location. Other locations such as 1, 6, and 7 in Figure 12(a) experience the torsional load. The effect of torsion is about 16 percent increase in the stress range at location 7.

Stress results obtained from the FE model were verified by experimental component test and strain gages. The differences between FEA and strain gage results were less than 7 percent for different loading conditions. This is an indication of the accuracy of the FE model used in this study. The FEA results indicated non-symmetric bending stresses on the crankpin bearing, whereas using analytical method predicts bending stresses to be symmetric at this location. The lack of stress symmetry is a geometry deformation effect, indicating the need for FEA modeling due to the relatively complex geometry of the crankshaft. The details of the experimental verification along with the finite element and analytical results are given in Montazersadgh and Fatemi (11).

More details of the FEA and discussion of results are provided in (11). As indicated earlier, even though only the modeling and analysis for the forged steel crankshaft are presented here, the same modeling and analysis were carried out for the ductile cast iron crankshaft, and similar results were obtained.

CRANKSHAFT FATIGUE TESTS AND COMPARISONS

To obtain and compare the fatigue performance of the two crankshafts, constant amplitude bending fatigue tests were performed.

Experimental Program

A cantilever bending fixture was designed to test the forged steel and cast iron crankshafts based on the critical (i.e. failure) location defined by FEA. Cantilever bending was used in order to minimize the magnitude of the applied loads necessary to achieve the desired nominal stresses. The schematic of the test set-up is shown in Figure 14. The same fixture was used for both crankshafts since their main journals were the same diameter.

As shown in Figure 14 the crankshaft was clamped into a support bar in the main journal section. The moment arm was clamped on the nose (front) main journal section. Load was applied through a rod end bearing in order to minimize the effects of misalignment. A rod fitted with roller bearings was attached to the rod end bearing. The rod end bearings were allowed to move in the slots of the moment arm. The bearings were necessary to minimize the friction in the fixture which would result in an axial load, when only bending was desired.

Tests were conducted on a 100 kN (22 Kip) closed-loop servo-hydraulic load frame controlled by a digital servo-controller. An applied R-ratio of -0.2 was used for all

tests, where R-ratio is defined as the ratio of the minimum to the maximum load. This R-ratio was identified from the dynamic loading analysis. Both crankshafts were tested at the same load (moment) amplitude due to similar in service loading conditions. The loads were selected to generate lives of 10^4 to 10^6 cycles for the forged steel crankshaft. Load frequencies between 1.4 and 3 Hz were used for all tests.

In order to help detect the initiation of cracks, each test was stopped at intervals corresponding to 10% to 20% of the expected life of the component. After a crack developed, its length was measured and recorded. The displacement amplitude was also monitored and recorded during each test to determine the change in displacement amplitude as the crack became longer.

Results and Comparisons

The results from the component fatigue tests are summarized in Table 3. Circumferential cracks developed in the crank-pin fillet that was identified by FEA as the critical location. Once a crack developed, the displacement amplitude increased and continued to increase as the crack grew longer. Eventually the displacement amplitude versus cycles reached an asymptotic value, at which point the crankshaft was considered to be fractured. The displacement amplitude versus cycles for the component fatigue tests are shown in Figure 15. Crack growth life of the component was a considerable portion of its fatigue life. Only several of the crankshafts were fractured, due to the considerable amount of time it took to grow the cracks through the section.

It was found that by the time the crack was able to be detected visually, it was already on the order of 5 mm (0.2 in) long. For life prediction purposes, initiation is defined as a crack on the order of 1 mm or 2 mm (0.04 in to 0.08 in). Therefore, the number of cycles when the crack was first observed was too large as crack initiation value. The fact that a crack will reduce the stiffness of a component and therefore cause a change in displacement amplitude was used to define crack initiation. The measured crack lengths and corresponding change in displacement amplitude values were used to develop a relationship between change in displacement and crack length for both crankshaft types. This information was extrapolated to a crack two 2 mm (0.08 in) in length. The resulting change in displacement amplitude was used as a measure for crack initiation. For comparison purposes, a 5% change in displacement amplitude was also used as an alternate failure criterion to the crack initiation criterion.

Moment amplitude versus cycles to failure using the crack initiation failure criterion is shown in Figure 16(a), while Figure 16(b) shows the moment amplitude versus cycles to failure using the 5% change in displacement amplitude criterion. Both plots of moment amplitude show that the forged steel crankshaft has better fatigue performance than the ductile cast iron crankshaft. The plot based on crack initiation shows that the forged steel crankshaft has a factor of 6 longer life than the cast iron crankshaft when tested at the same moment amplitude. The plot based on a 5% change in displacement amplitude shows that the difference in lives is less at short lives and greater at long lives. The plot shows that at long lives there is approximately an order of magnitude difference in fatigue lives.

A fatigue limit was also observed with the forged steel crankshaft around 10^6 cycles. As expected, the moment versus life to failure plots suggest that the cast iron crankshaft does not have a fatigue limit at 10^6 cycles. The results from the tests show that the forged steel crankshaft has a fatigue limit of 413 N-m (305 lb-ft), below which failure should not occur. The ductile cast iron crankshaft has a fatigue strength of 315

N-m (232 lb-ft) at 10^6 cycles. The fatigue strength at 10^6 cycles for the cast iron crankshaft was 76% of the forged steel, which compares to the difference observed between the fatigue strength at 10^6 cycles from the specimen tests, where the cast iron fatigue strength was 73% of the forged steel.

Typical fracture fractures for the forged steel crankshaft are shown in Figure 17(a) and for the cast iron crankshaft in Figure 17(b). The figures show that the forged steel fracture surface is smoother than the cast iron, as expected due to the greater ductility in the forged steel. The figures also show that the crack grew through the circular cross-section for the cast iron crankshaft, but the crack in the forged steel crankshaft started in the crankpin fillet and then grew through the web section. Figure 17(b) shows the eccentricity of the hole in the cast iron crankshaft, where the wall thickness is the greatest was the location of the highest stress. More details of the crankshaft fatigue tests and discussion of the obtained results are provided in (9).

FATIGUE LIFE PREDICTIONS

Due to the long life situation of a crankshaft, the S-N approach is commonly used. The fatigue notch factor K_f at the fillet was determined using the stress concentration factor along with Peterson's equation (12) given by:

$$K_f = 1 + \frac{K_t - 1}{1 + a/r} \tag{6}$$

where K_t is the stress concentration factor, r is the radius of the notch and a is the material characteristic length. The stress concentration factor, K_t, for both crankshafts was determined by FEA. The fatigue strength at 2 x 10^6 reversals was reduced by K_f, to determine the S-N line for the notched condition. To account for the R ratio of -0.2 instead of R = -1, the Modified Goodman equation (12) represented by:

$$\frac{S_a}{S_{Nf}} + \frac{S_m}{S_u} = 1 \tag{7}$$

was used, where S_a is the stress amplitude, S_m is the mean stress, S_u is the ultimate strength of the material, and S_{Nf} is the notched fatigue strength at 2 x 10^6 reversals for fully reversed loading. More details of the fatigue life predictions are given by Williams and Fatemi in (9).

The results from the S-N life predictions are summarized along with the component fatigue test data in Table 3. Figure 18 shows a plot of predicted cycles to failure versus experimental cycles to failure (based on initiation) for the S-N approach along with scatter bands at ± 2 and ± 3. The plot shows that the predicted cycles to failure were within a factor of two for the forged steel crankshaft. The predicted cycles to failure for the ductile cast iron crankshaft were not as accurate but were conservative. Similar results were obtained when the 5% change in displacement amplitude failure criterion was used.

OPTIMIZATION

In this study reducing the weight and manufacturing cost and improving fatigue performance of the crankshaft were the main objectives of the optimization study. Material mechanical properties are the first constraints that limit the stress levels at different locations. Other applied constraints were based on the fact that the optimized crankshaft should be replaceable with the current one. This results in geometry restrictions mainly for the crank radius, outer diameters of bearings, their distances, and dimensions of different steps on the shaft.

Optimization variables consisted of three categories related to geometry, manufacturing process, and using alternative materials. Geometry variables were thickness of the crank web, geometry of the crank web, changing the inner hole diameters and their depths, and geometry changes on outer part of connecting rod bearing. Manufacturing variables included modification to the current production process according to geometry changes as well as inducing compressive residual stress at the fillets, which are the critical (i.e. failure) locations, by processes such as fillet rolling. Using alternative materials such as microalloyed steels can result in better performance while reducing the cost of the forged steel crankshaft by eliminating the heat treating process.

It should be noted that the optimization carried out on this component is not the typical mathematical sense of optimization, because all variables cannot be represented in a mathematical function according to the set of constraints such that the maximum or minimum could be obtained. Instead, the judgment is based on mass reduction, cost reduction, and improving fatigue performance using alternative materials and considering manufacturing aspects.

Local geometry optimization was applied separately to different sections of the crankshaft based on the results of dynamic load and stress analysis. The first local optimization is increasing the depth of the back hole from 33 mm to 114 mm (1.3 in to 4.50 in). Increasing the oil hole diameter of the crankpin from 18.3 mm to 22.4 mm (0.72 in to 0.88 in) was another optimization option considered. Since the stresses increase in the fillet area due to this diameter increase, the fillet radius was modified from 2.38 mm to 3.18 mm (3/32 in to 4/32 in). Reducing the web thickness by 3.81 mm (0.15 in) from each web was considered as the next step of geometry optimization. Changing the geometry of the web, as can be seen in Figure 19, also reduced the weight of the component further.

These different optimization potentials were considered, having confirmed their feasibility in manufacturing, cost and stress they were combined and the dynamic load and stress analysis was applied to the alternative geometry. The final optimized geometry is shown in Figure 19, along with the original crankshaft showing locations where local optimization has been applied. The result of the geometry optimization process is 12% weight reduction compared with the original crankshaft. Dynamic and FE analysis on the final optimized crankshaft shows the same stress range at the critical location, as in the original crankshaft. With regards to stiffness, the maximum displacement increases by only 15% as compared to the original crankshaft, which is reasonable since the displacements due to the applied stresses are on the order of 10^{-2} mm.

Residual stress in the fillet area of the crankshaft can significantly improve the fatigue strength of the component. Park et al. (13) showed that without any dimensional modification, one can significantly improve the fatigue life of crankshaft by applying fillet rolling. The experimental data from their study indicates that surface modification can

dramatically increase endurance life of crankshafts. The fillet rolled crankshaft at 900 kgf showed more than 80% increase in fatigue limit, while the fillet rolled crankshaft at 500 kgf sample exhibited improvement of 40% in the fatigue limit.

The geometry of the crankshaft could be modified even further to take advantage of the results of improved fatigue strength of the component from fillet rolling. Increasing the crankpin hole diameter is a cost effective option which does not influence the manufacturing process. Increasing the bore diameter from 18.3 mm to 25.4 mm (0.72 in to 1 in) will cause the stress range at the critical location to increase by 7%. This stress increase can easily be covered by the significant beneficial effect of the compressive residual stress from fillet rolling. Since the wall thickness in the crankpin area is limited, further increasing the bore diameter is, however, not possible because sufficient material is needed to restrict plastic deformation during the rolling process. This additional modification will reduce the weight of the original crankshaft by a total of 18%. In addition, fatigue performance improvement considering the residual stress is about 165%.

A common alternative for the forged steel material is micro-alloyed steel. Pichard et al. (1) performed a study on a microalloyed (MA) steel with titanium addition specially adapted for the production of forged crankshafts and which does not require any post-forging treatment. The use of MA steel enables elimination of any further heat treatment, resulting in shorter manufacturing process and consequently an increase in the forged crankshaft productivity. The metallurgical choice of this MA steel for crankshaft applications was based on the 35MV7 steel grade, with a typical composition of 0.35C, 1.8Mn, 0.25Si, 0.12V, and micro-addition of Ti. A comparison between the material properties used in the current crankshaft, AISI 1045, and MA steel 35MV7 indicates similar yield strengths, 12% higher tensile strength, and slightly lower fatigue strength (by 6%) at 10^7 cycles for the MA steel.

With regards to cost, although the use of MA steel results in slightly higher raw material cost as compared to the current steel, the savings due to the elimination of the heat treatment (quenching and tempering) are far greater. In addition, MA steel has 5% to 10% better machinability than the current steel. Considering these factors, along with the reduced material cost due to the 18% weight reduction indicates significant reduction in the total cost of the forged steel crankshaft.

CONCLUSIONS

Material and component fatigue tests and life predictions, along with FEA, and dynamic analysis were performed on forged steel and ductile cast iron crankshafts. An optimization study was also carried out for the forged steel crankshaft. Based on the experimental results and the analyses performed, the following conclusions can be drawn:

1. The ultimate strength and yield strength of the ductile cast iron material were 66% and 80% of the forged steel, respectively. The forged steel also showed significantly more ductility than the ductile cast iron as shown by the percent reduction in area of 58% for forged steel and 6% for the cast iron.
2. The S-N curves for the two materials show that the fatigue strength at 10^6 cycles for forged steel and ductile cast iron were 359 MPa and 263 MPa, respectively. This results in the forged steel material having a factor of 30 longer life than the ductile cast iron in the high cycle region.

3. Comparison of the Neuber curves for the two materials shows that when tested at the same Neuber stress range, the forged steel has a factor of 50 longer life than the ductile cast iron.
4. Both L-T and T-L Charpy V-notch specimen orientations for the forged steel had significantly higher impact toughness than the cast iron specimens at all temperature levels tested.
5. Dynamic loading analysis of the crankshaft results in more realistic stresses whereas static analysis provides an overestimate results. Accurate stresses are critical input to fatigue analysis and optimization of the crankshaft.
6. Considering torsional load in the overall dynamic loading conditions has no effect on von Mises stress at the critically stressed location. The effect of torsion on the stress range is also relatively small at other locations undergoing torsional load.
7. Experimental and FEA results showed close agreement, within 7% difference. FEA results indicate non-symmetric bending stresses on the crankpin bearing, whereas using analytical method predicts bending stresses to be symmetric at this location. The lack of symmetry is a geometry deformation effect, indicating the need for FEA modeling due to the relatively complex geometry of the crankshaft.
8. Crack growth life was a significant portion of the fatigue life of both crankshafts. The crack growth rate of the forged steel crankshaft was slower than the ductile cast iron crankshaft.
9. When tested at the same moment amplitude the forged steel crankshaft had 32% higher fatigue strength at a million cycles, compared the ductile cast iron crankshaft. This resulted in a factor of 6 longer life for the forged steel crankshaft when the crack initiation failure criterion was used. The difference in lives is even greater when the 5% change in displacement amplitude criterion is used.
10. Life predictions using the S-N approach provided reasonable estimations of the fatigue lives for both the forged steel and ductile cast iron crankshafts, although it was more accurate with the forged steel.
11. Geometry optimization resulted in 18% weight reduction of the forged steel crankshaft. Adding fillet rolling in the manufacturing process also results in 165% increase in fatigue strength of the crankshaft.
12. Using MA steel as an alternative material to the current forged steel results in the elimination of the heat treatment leading to significant cost savings. Considering better machinability of the MA steel along with the reduced material cost due to the 18% weight reduction result in significant reduction in overall cost of the forged steel crankshaft.

REFERENCES

1. Pichard, C., Tomme, C., and Rezel, D., 1993 “Alternative Materials for the Manufacture of Automobile Components: Example of Industrial Development of a Microalloyed Engineering Steel for the Production of Forged Crankshafts,” In *Proceedings of the 26th ISATA International Symposium on Automotive Technology and Automation*, Aachen, Germany.

2. Chatterley, T.C. and Murrell, P., 1998, “ADI Crankshafts- An Appraisal of Their Production Potentials,” *SAE Technical Paper No. 980686*, Society of Automotive Engineers.

3. Jensen, E. J., 1970, “Crankshaft strength through laboratory testing,” *SAE Technical Paper* No. 700526, Society of Automotive Engineers.

4. Chien, W.Y., Pan, J., Close, D., and Ho, S., 2005, “Fatigue Analysis of Crankshaft Sections Under Bending with Consideration of Residual Stresses,” *International Journal of Fatigue*, Vol. 27, pp. 1-19.

5. Zoroufi, M. and Fatemi, A, 2005, “A Literature Review of Durability Evaluation of Crankshafts Including Comparisons of Competing Manufacturing Processes and Cos Analysis,” *26th Forging Industry Technical Conference*, Chicago, IL.

6. ASTM Standard E606-92, “Standard Practice for Strain-Controlled Fatigue Testing,” *Annual Book of ASTM Standards*, Vol. 03.01, 2004.

7. ASTM Standard E8-04, “Standard Test Methods for Tension Testing of Metallic Materials,” *Annual Book of ASTM Standards*, Vol. 03.01, 2004.

8. ASTM Standard E23-02a, “Standard Test Methods for Notched Bar Impact Testing of Metallic Materials,” *Annual Book of ASTM Standards*, Vol. 03.01, 2004.

9. Williams, J. and Fatemi, A., 2007, “Fatigue Performance of Forged Steel and Ductile Cast Iron Crankshafts”, *SAE Technical Paper* No. 2007-01-1001, Society of Automotive Engineers.

10. Fergusen, C. R., 1986, “*Internal Combustion Engines, Applied Thermo Science*,” John Wiley and Sons, New York, NY, USA.

11. Montazersadgh, F. and Fatemi, A., 2007, “Dynamic Load and Stress Analysis of a Crankshaft,” *SAE Paper No. 2007-01-0258*, Society of Automotive Engineers.

12. Stephens, R.I., Fatemi, A., Stephens, R.R., and Fuchs, H.O., 2001, “*Metal Fatigue in Engineering*,” 2nd Edition, John Wiley & Sons, Inc., New York, New York, USA.

13. Park, H., Ko, Y. S., and Jung, S. C., 2001, “Fatigue Life Analysis of Crankshaft at Various Surface Treatments,” *SAE Technical Paper* No. 2001-01-3374, Society of Automotive Engineers.

Table 1: Monotonic and cyclic properties for the forged steel and ductile cast iron materials.

Monotonic Properties	Forged Steel	Cast Iron	Ratio
Average Hardness, HRC	23	18	0.8
Average Hardness, HRB	101	97	0.96
Modulus of Elasticity, E, Gpa	221	178	0.81
Yield Strength (0.2%offset), YS, MPa	625	412	0.66
Ultimate Strength, S_u, Mpa	827	658	0.80
Percent Elongation, %EL	54%	10%	0.19
Percent Reduction in Area, %RA	58%	6%	0.10
Strength Coefficient, K, MPa	1316	1199	0.91
Strain Hardening Exponent, n	0.152	0.183	1.20
True Fracture Strength, σ_f, MPa	980	562	0.57
True Fracture Ductility, ε_f	87%	6%	0.07

Cyclic Properties	Forged Steel	Cast Iron	Ratio
Fatigue Strength Coefficient, σ_f', MPa	1124	927	0.82
Fatigue Strength Exponent, b	-0.079	-0.087	1.10
Fatigue Ductility Coefficient, ε_f'	0.671	0.202	0.30
Fatigue Ductility Exponent, c	-0.597	-0.696	1.17
Cyclic Yield Strength, YS', MPa	505	519	1.03
Cyclic Strength Coefficient, K', MPa	1159	1061	0.91
Cyclic Strain Hardening Exponent, n'	0.128	0.114	0.89
Fatigue Strength at $N_f=10^6$, MPa	359	263	0.73

Note: Forged steel taken as the base for all ratio calculations

Table 2: Configuration of the engine to which the crankshaft belongs.

Crankshaft radius	37 mm
Piston Diameter	89 mm
Mass of the connecting rod	0.283 kg
Mass of the piston assembly	0.417 kg
Connecting rod length	120.78 mm
I_{zz} of connecting rod about the center of gravity	0.663×10^{-3} kg-m^2
Distance of C.G. of connecting rod from crank end center	28.6 mm
Maximum gas pressure	35 Bar

Table 3: Results of component fatigue tests and S-N life predictions.

Applied Moment Amp. (N-m)	Cycles at First Observed Crack	Crack Initiation from Fitted Data	Cycles at 5% Change in Disp. Amp.	S-N Prediction
Forged Steel Crankshaft				
630	--	29,248	45,568	49,719
	--	45,302	69,670	49,719
	--	58,236	90,853	49,719
517	165,000	145,000	234,289	182,712
	120,000	98,741	213,885	182,712
	--	204,174	396,011	182,712
431	>2,090,000	>2,090,000	>2,090,000	>1,000,000
	>3,980,000	>3,980,000	>3,980,000	>1,000,000
350	>3,240,000	>3,240,000	>3,240,000	>1,000,000
Cast Iron Crankshaft				
630	11,504	7,132	17,353	2,900
	11,692	9,256	17,380	2,900
	8,021	8,021	20,957	2,900
517	31,464	25,512	47,513	12,252
	34,898	24,096	52,790	12,252
	42,750	37,380	54,966	12,252
431	113,043	75,200	132,877	43,601
	90,175	78,367	121,866	43,601
	--	82,200	143,259	43,601
350	985,496	920,783	1,005,665	178,214
	--	301,774	370,216	178,214

(a) (b)

Figure 1: (a) Forged steel crankshaft and (b) ductile cast iron crankshaft.

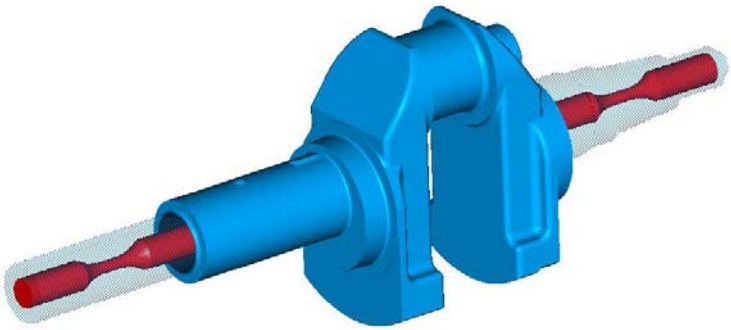

(a)

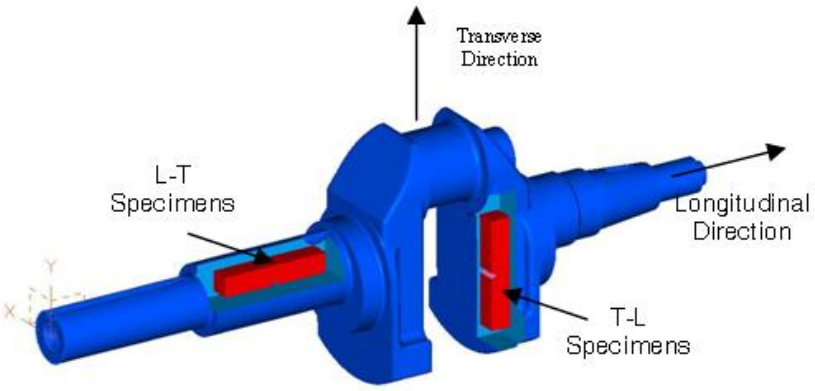

(b)

Figure 2: (a) Specimen orientation for monotonic and fatigue specimen tests, and (b) orientation of Charpy V-notch specimens.

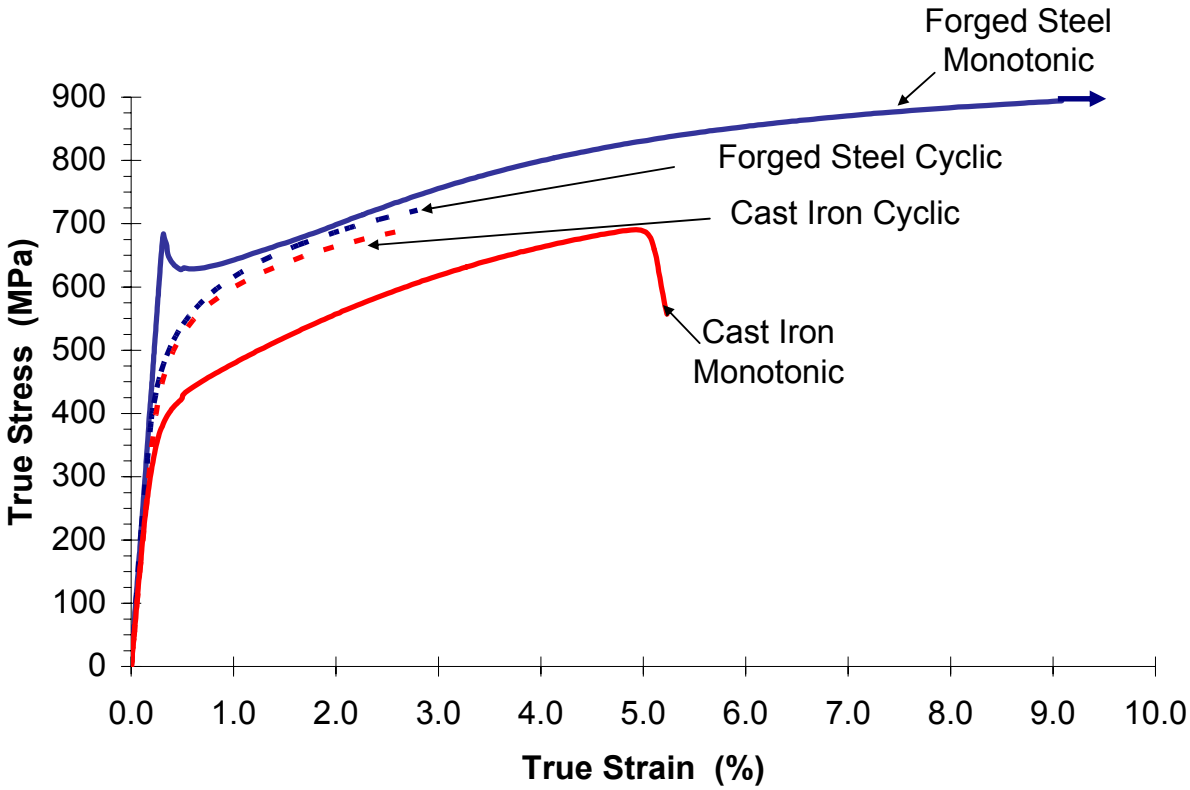

Figure 3: Superimposed plots of monotonic and cyclic stress-strain curves for the forged steel and ductile cast iron materials.

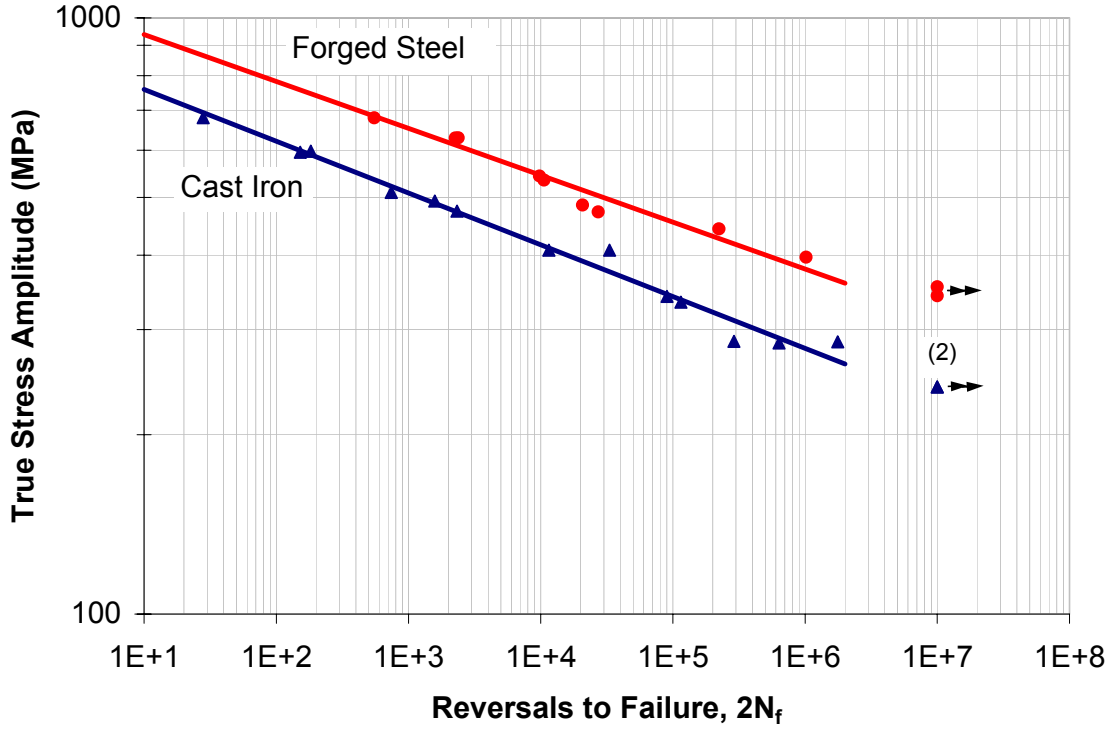
1000
100
Forged Steel
Cast Iron
(2)
True Stress Amplitude (MPa)
1E+1
1E+2
1E+3
1E+4
1E+5
1E+6
1E+7
1E+8
Reversals to Failure, 2N$_f$

(a)

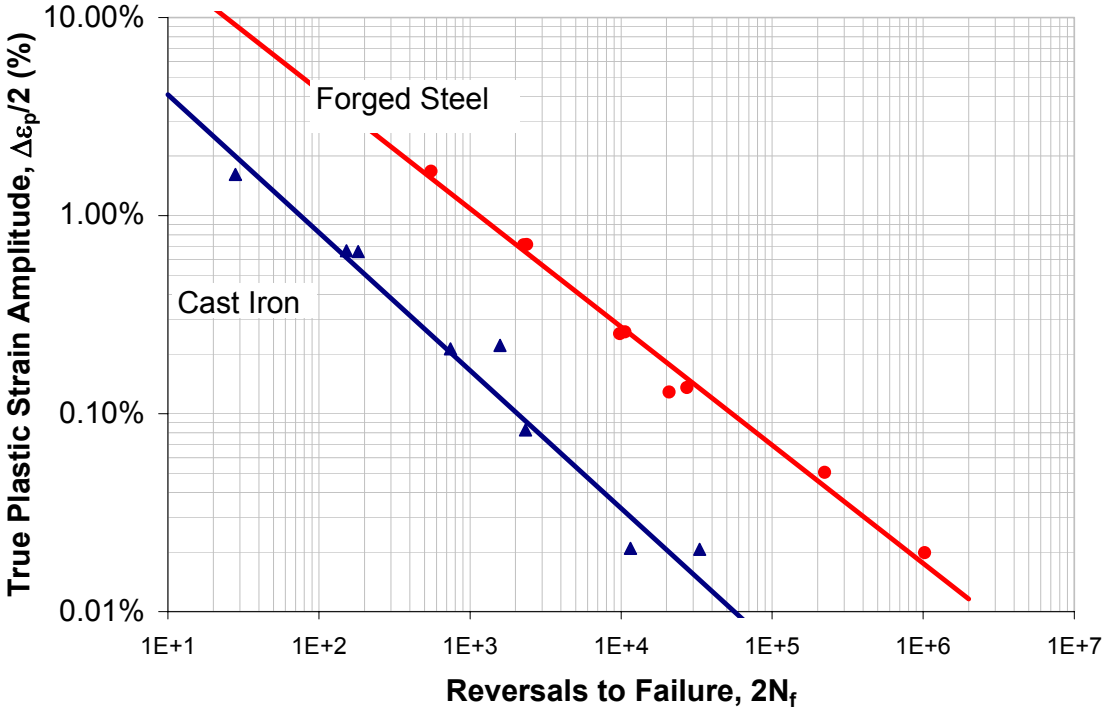
10.00%
1.00%
0.10%
0.01%
Forged Steel
Cast Iron
True Plastic Strain Amplitude, Δε$_p$/2 (%)
1E+1
1E+2
1E+3
1E+4
1E+5
1E+6
1E+7
Reversals to Failure, 2N$_f$

(b)

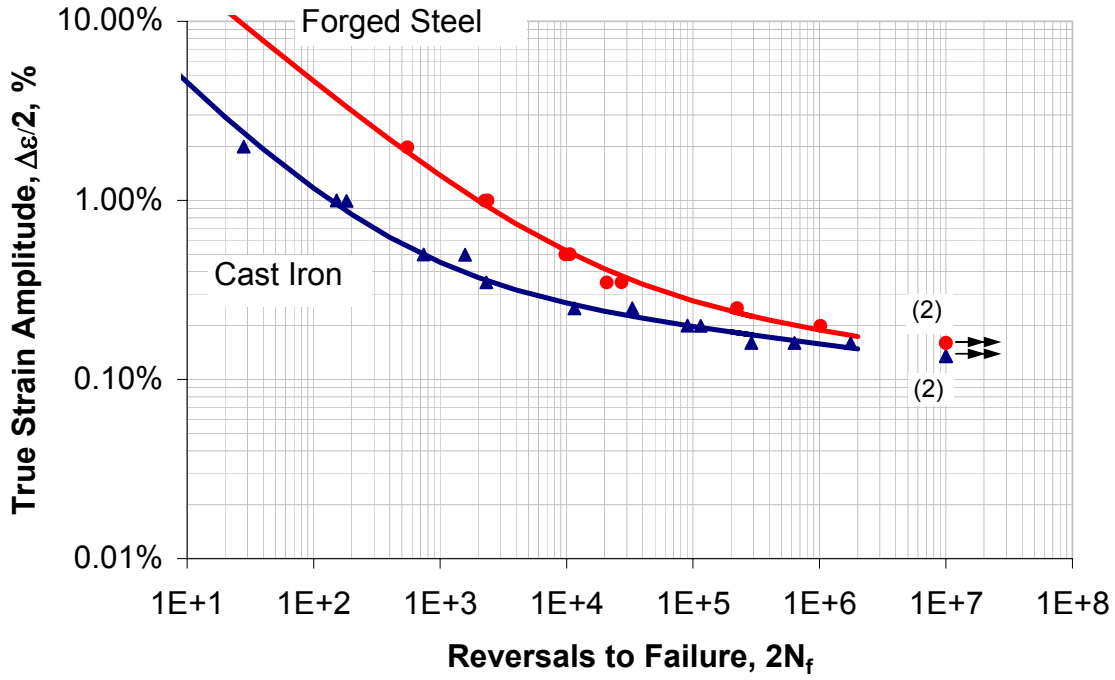

(c)

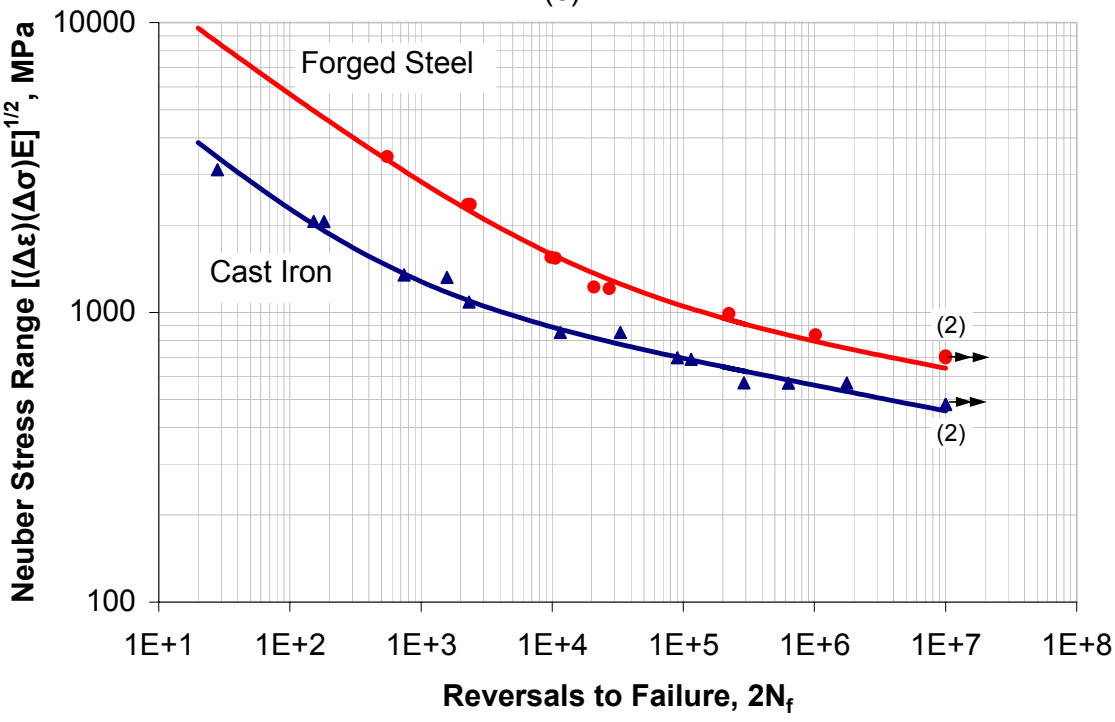

(d)

Figure 4: (a) True stress amplitude versus reversals to failure, (b) true plastic strain versus reversals to failure, (c) true strain amplitude versus reversals to failure, and (d) Neuber stress range versus reversals to failure for the forged steel and ductile cast iron materials.

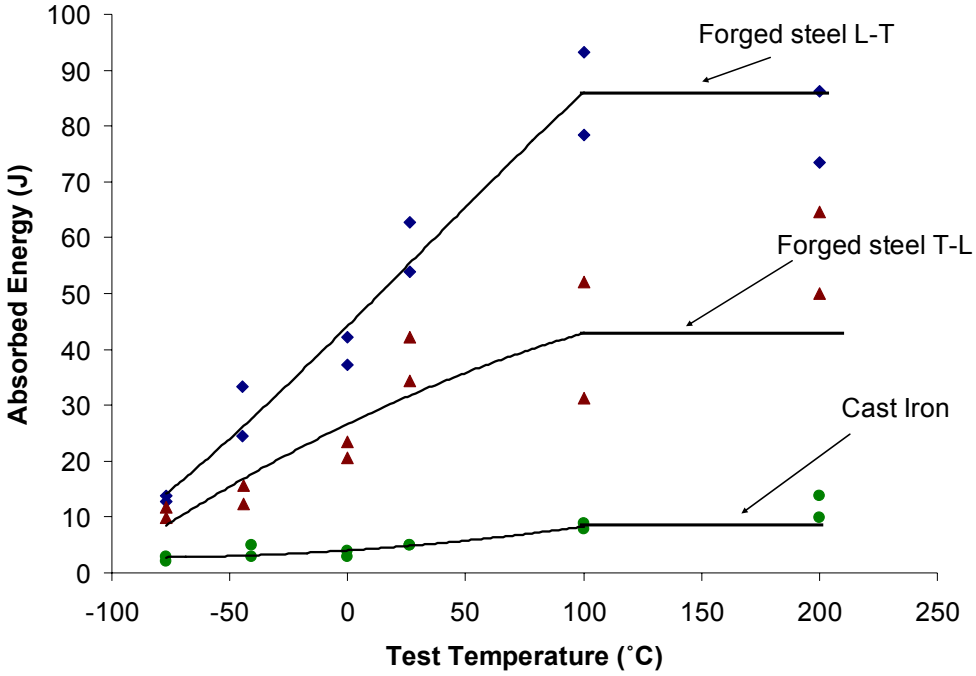

(a)

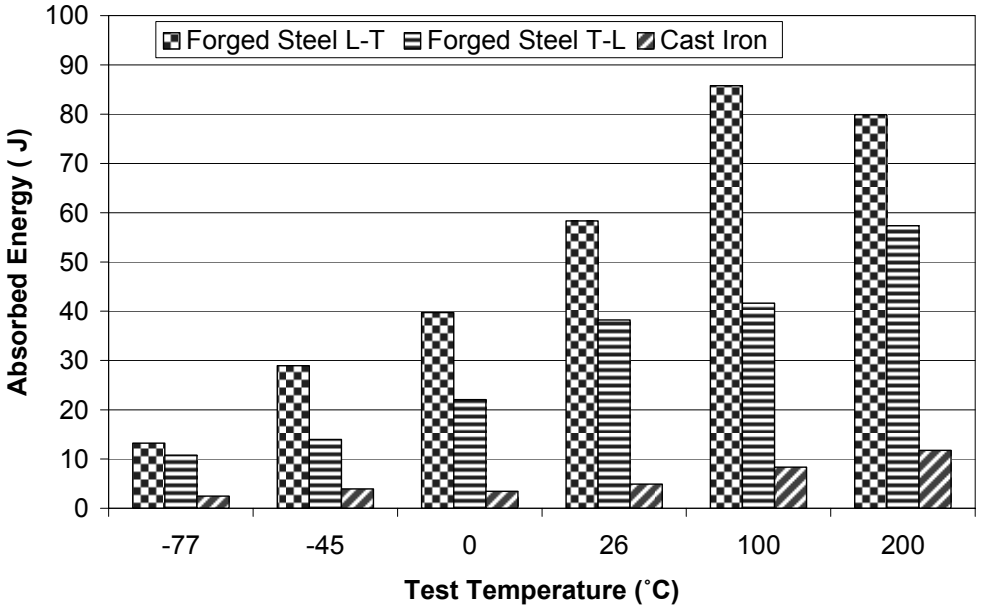

(b)

Figure 5: Absorbed energy values at the six temperature levels for the L-T and T-L forged steel and the cast iron Charpy specimens. Individual test results are shown in (a) and average values in (b).

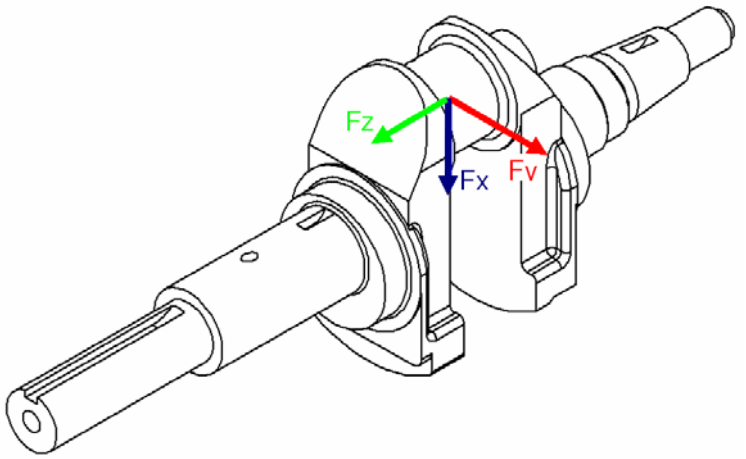

Figure 6: Crankshaft geometry and bending (F_x), torsional (F_y), and longitudinal (F_z) force directions.

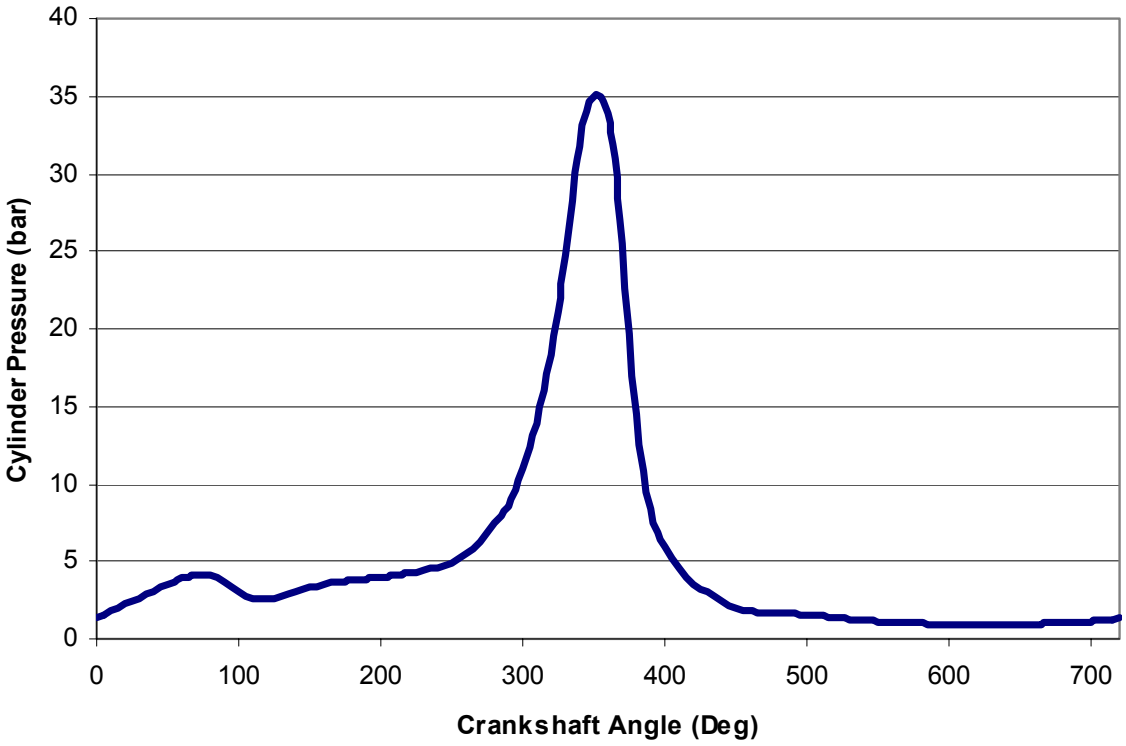

Figure 7: Piston pressure versus crankshaft angle diagram used to calculate forces at the connecting rod ends.

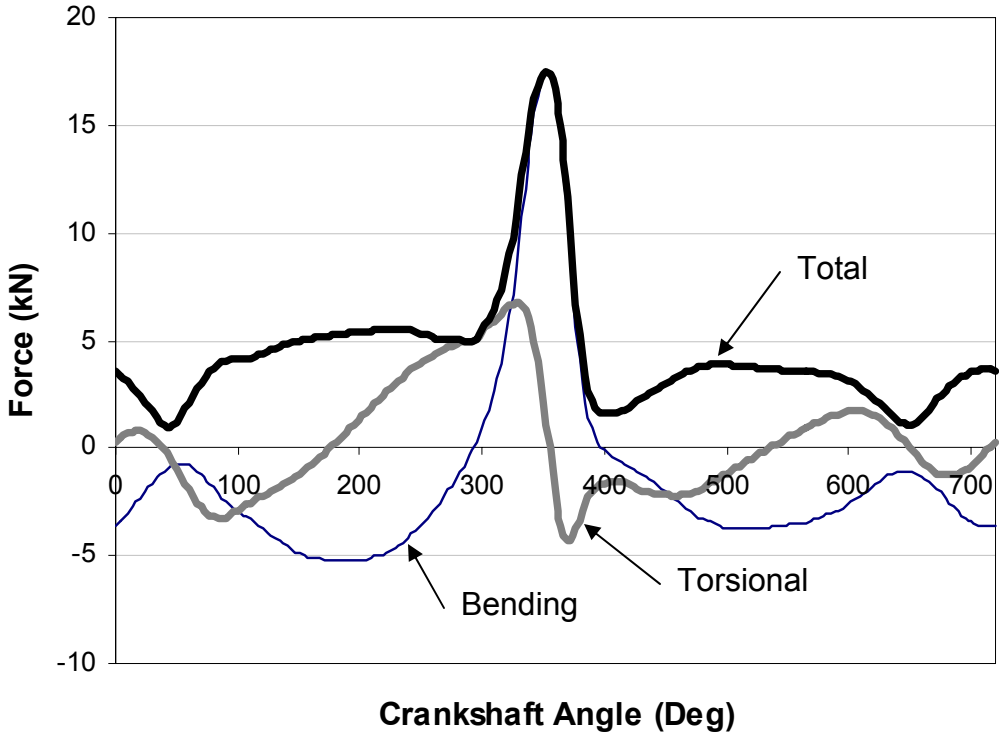

Figure 8: Bending, torsional, and the resultant force at the connecting rod bearing at the engine speed of 3600 rpm.

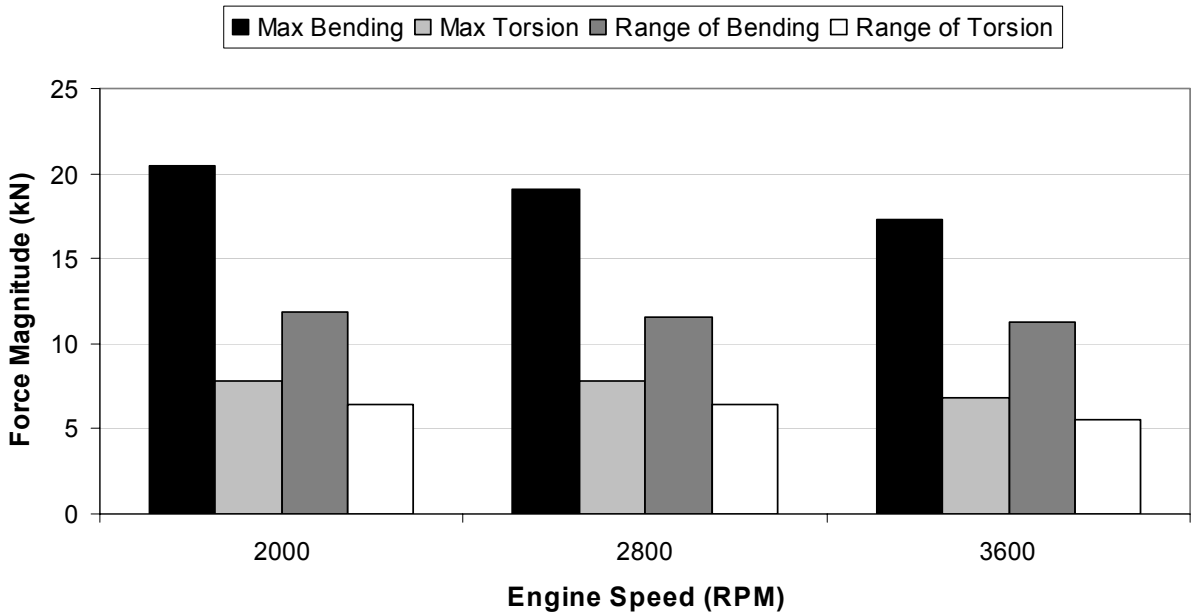

Figure 9: Comparison of maximum and range of bending and torsional loads at different engine speeds.

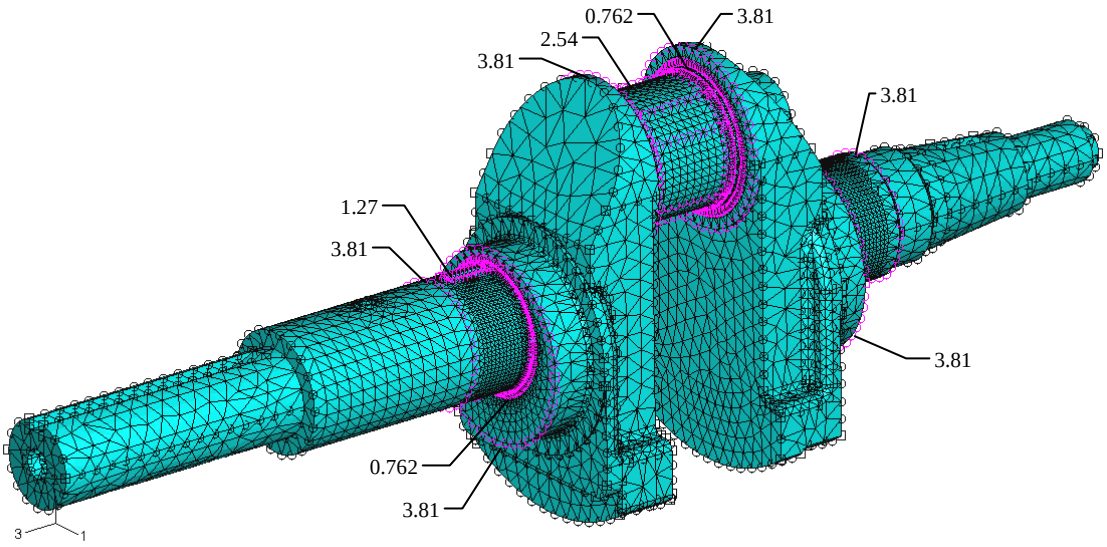

Figure 10: Element size at different locations on the forged steel crankshaft geometry.

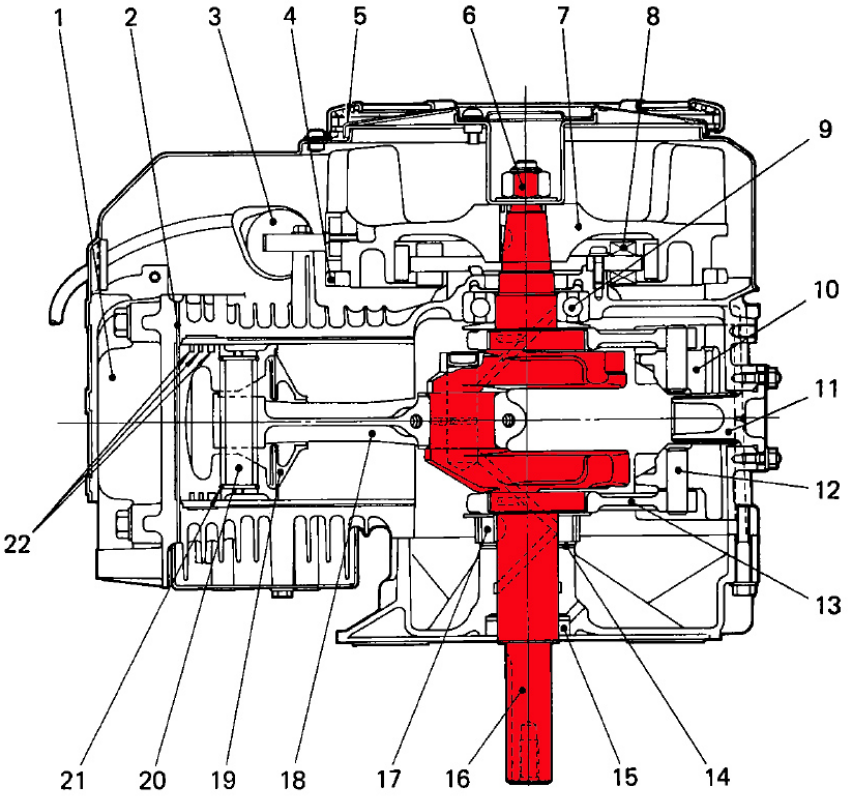

(a)

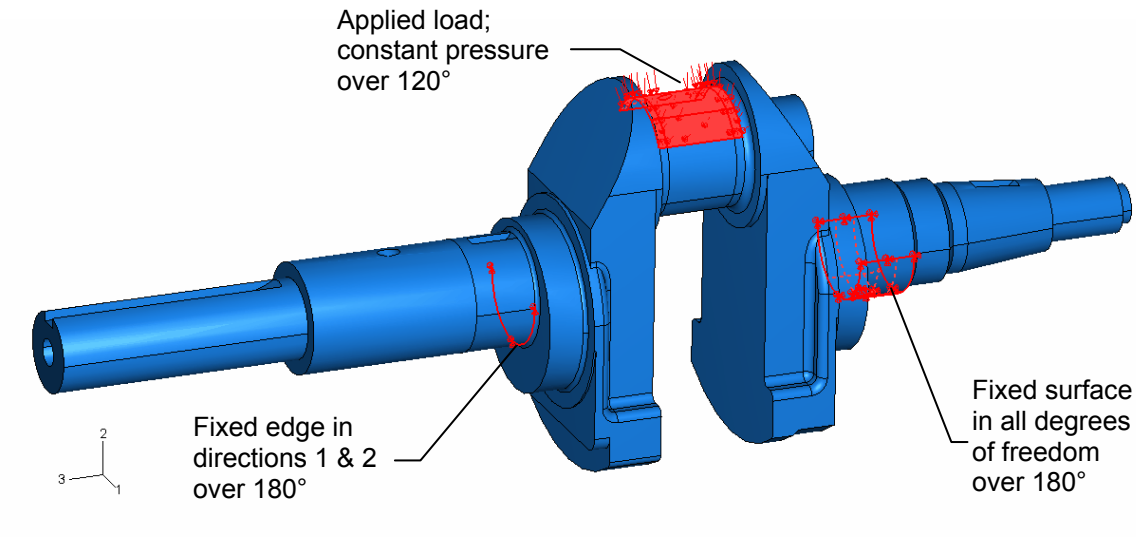

(b)

Figure 11: Crankshaft position in the engine block (a) and one step of the boundary conditions used in the FEA model (b).

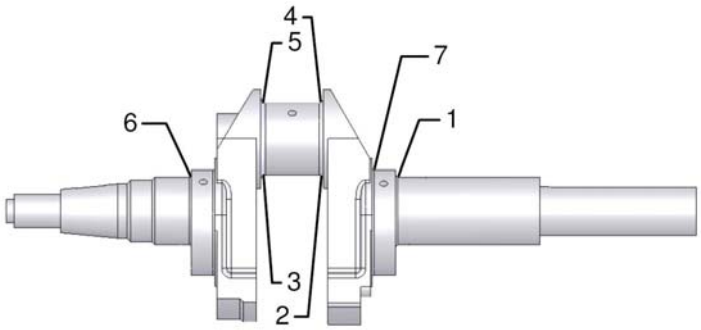
4
5
7
6
1
3
2

(a)

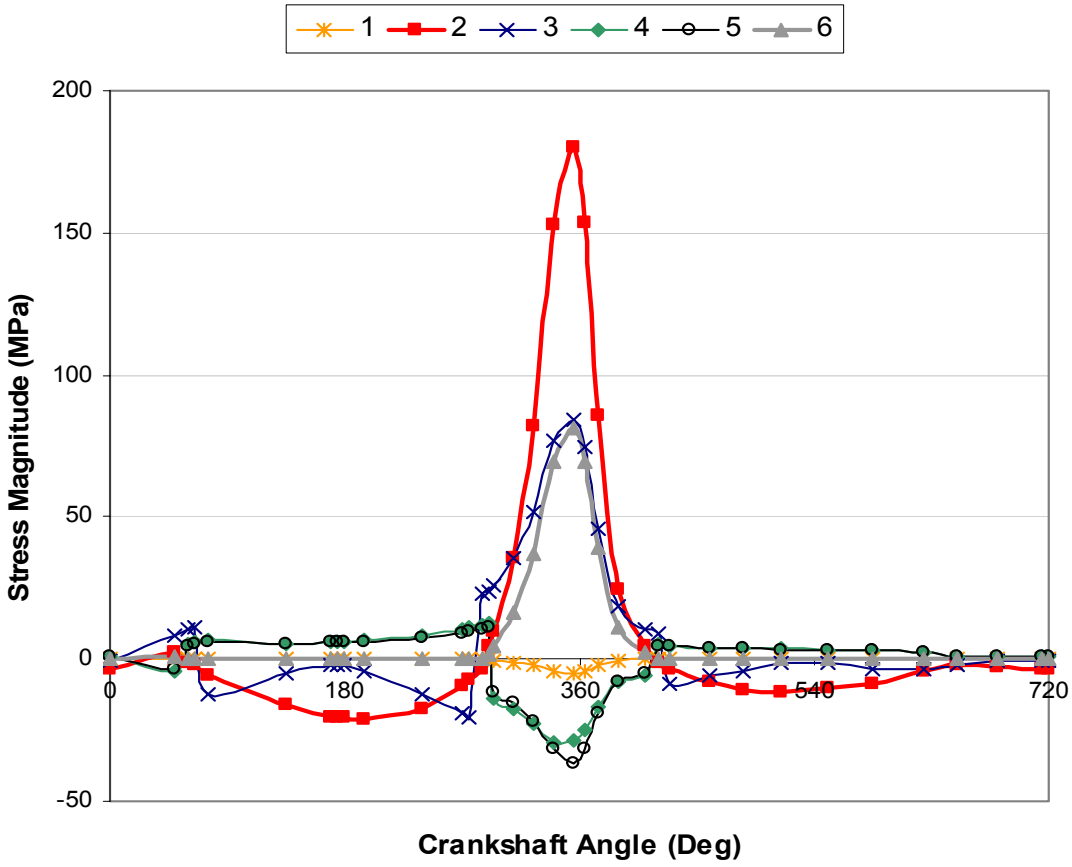
1
2
3
4
5
6
200
150
100
50
0
-50
Stress Magnitude (MPa)
0
180
360
540
720
Crankshaft Angle (Deg)

(b)

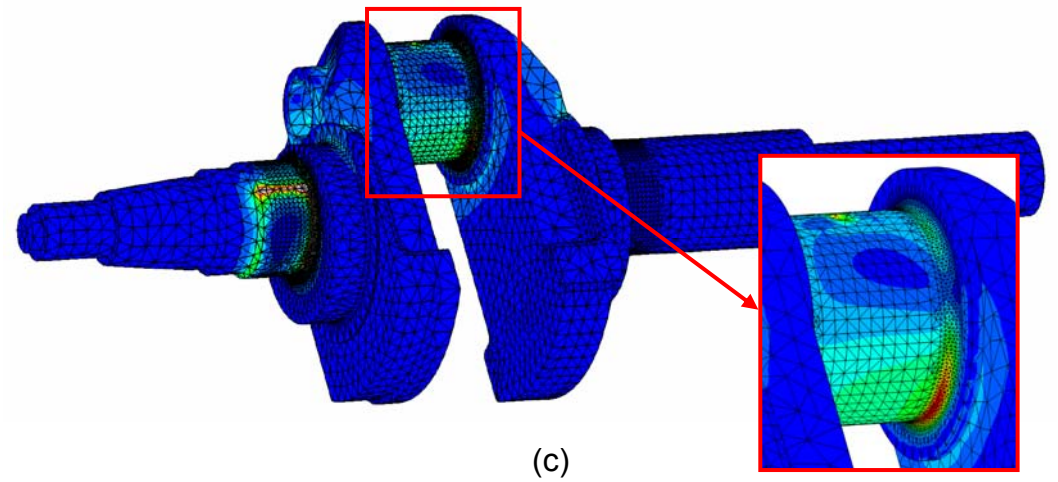

(c)

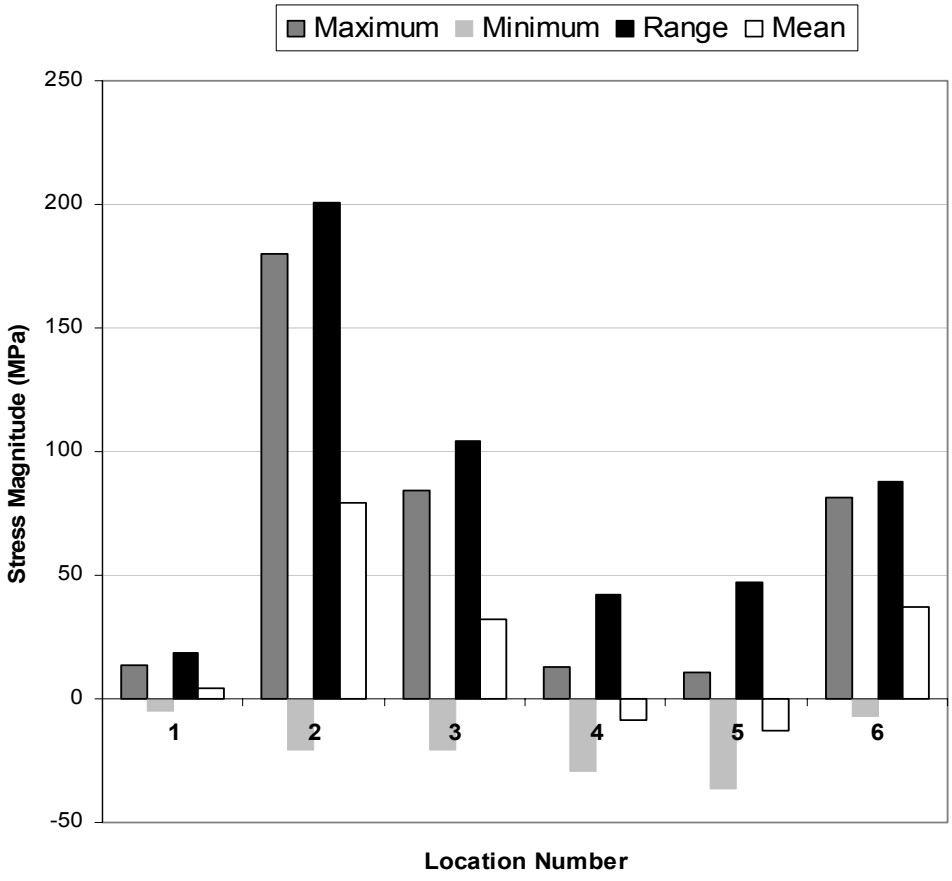

(d)

Figure 12: (a) Locations on the crankshaft where the stress variation was traced over one cycle of the engine. (b) von Mises stress history (considering sign of principal stress) at different locations at engine speed of 2000 rpm. (c) von Mises stress contour for forged steel crankshaft. (d) Comparison of maximum, minimum, mean, and range of stress at engine speed of 2000 rpm at different locations on the forged steel crankshaft.

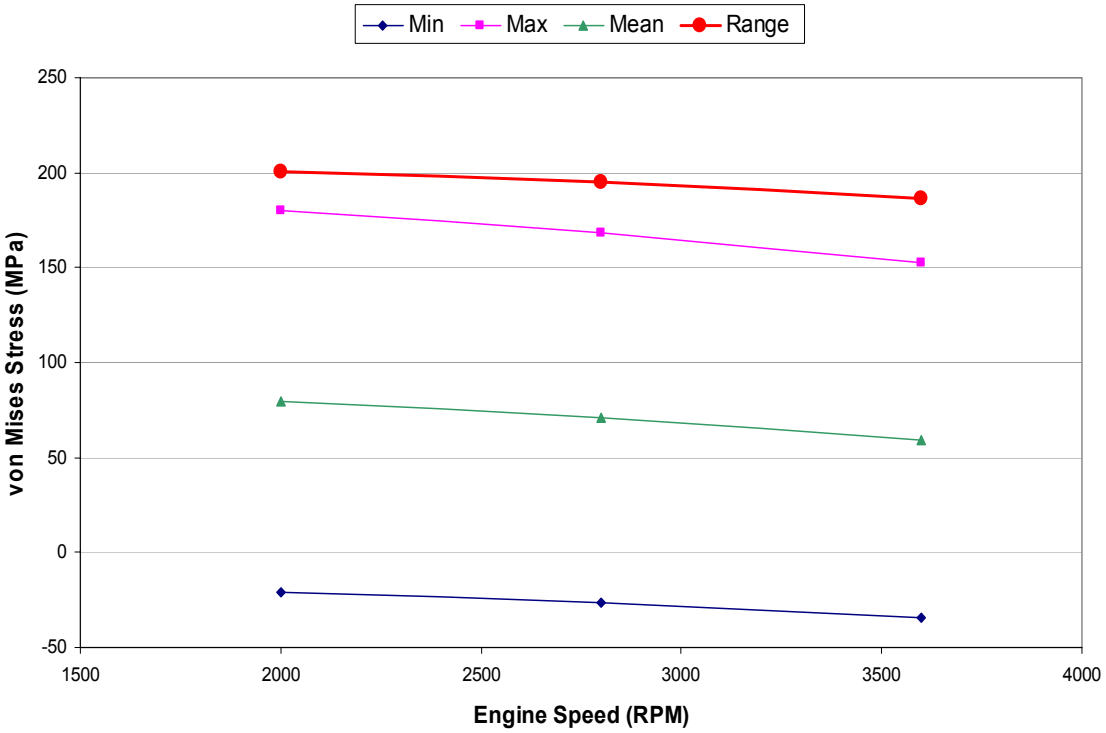

Figure 13: Variation of minimum stress, maximum stress, mean stress, and stress range at location 2 on the forged crankshaft as a function of engine speed.

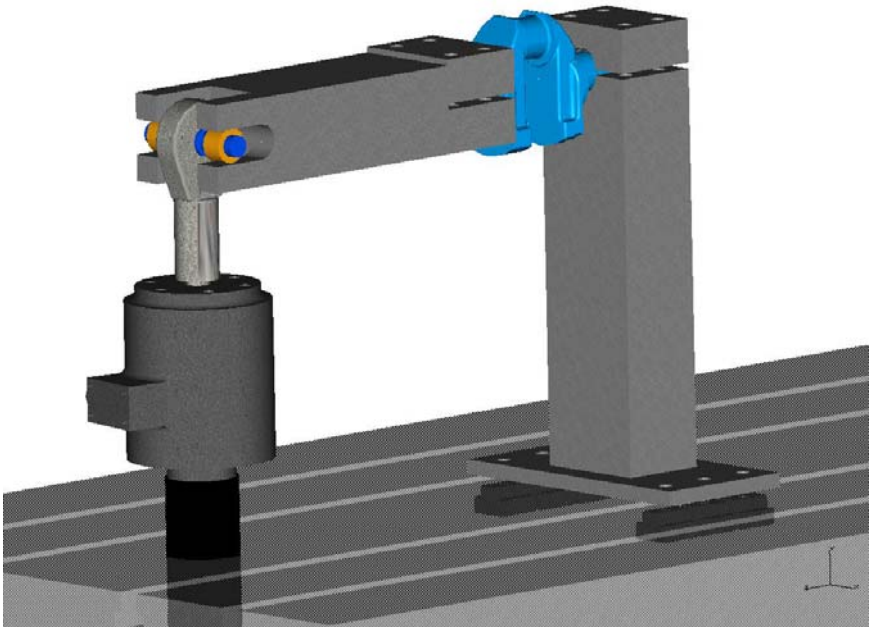

Figure 14: Schematic of crankshaft fatigue test setup.

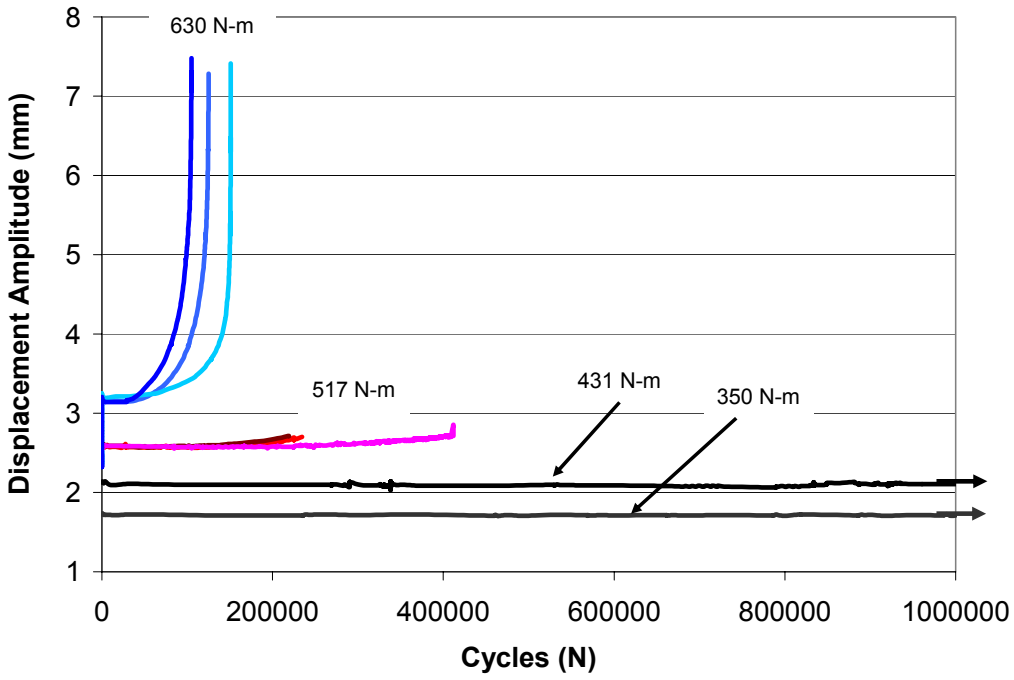

(a)

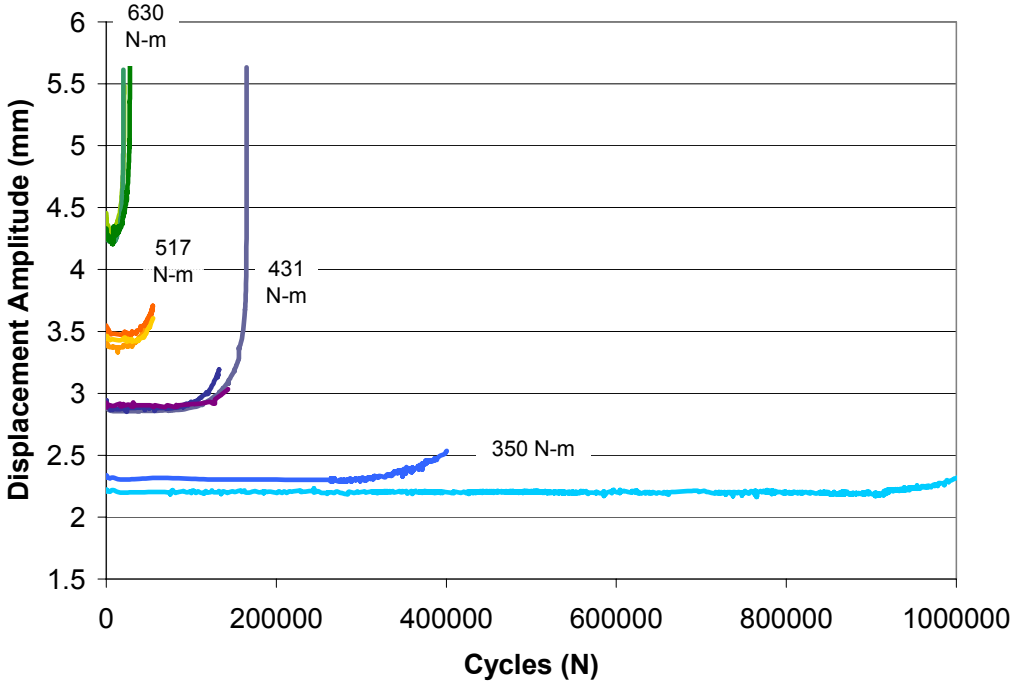

(b)

Figure 15: Displacement amplitude versus cycles for the (a) forged steel and (b) cast iron crankshafts.

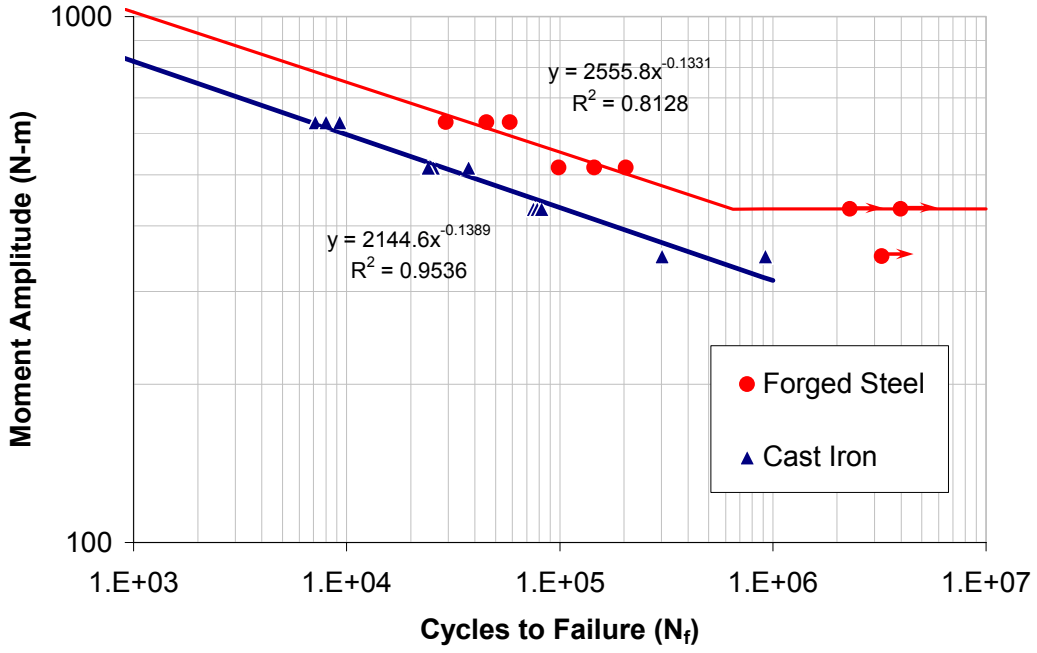

(a)

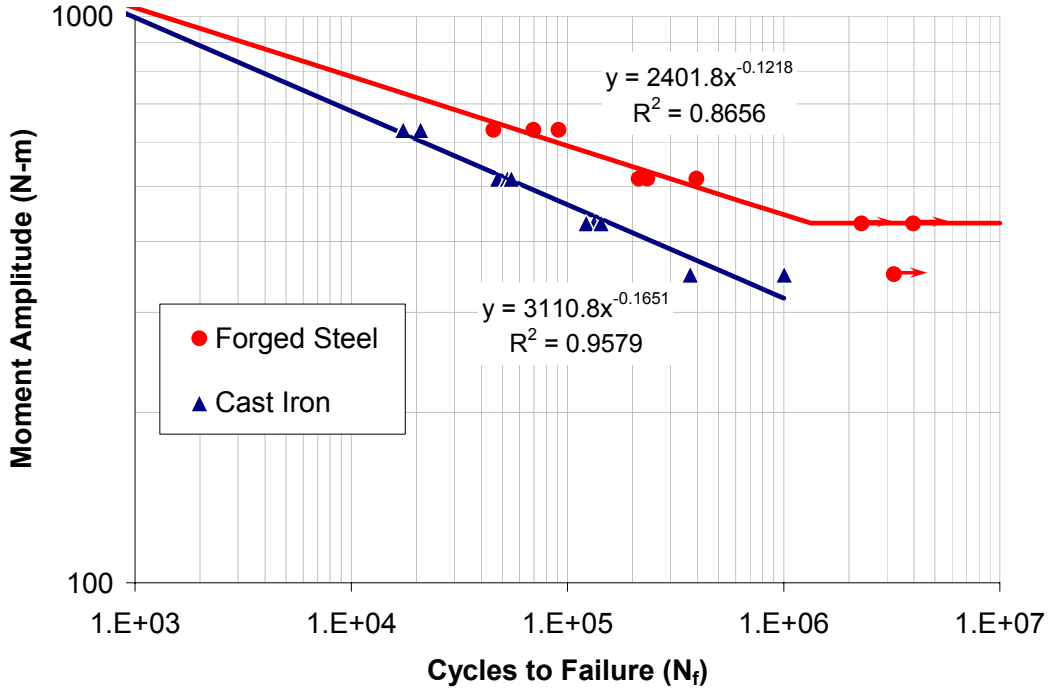

(b)

Figure 16: Moment amplitude versus cycles to failure for the component fatigue tests using (a) the crack initiation failure criterion, and (b) using the 5% change in displacement amplitude failure criterion.

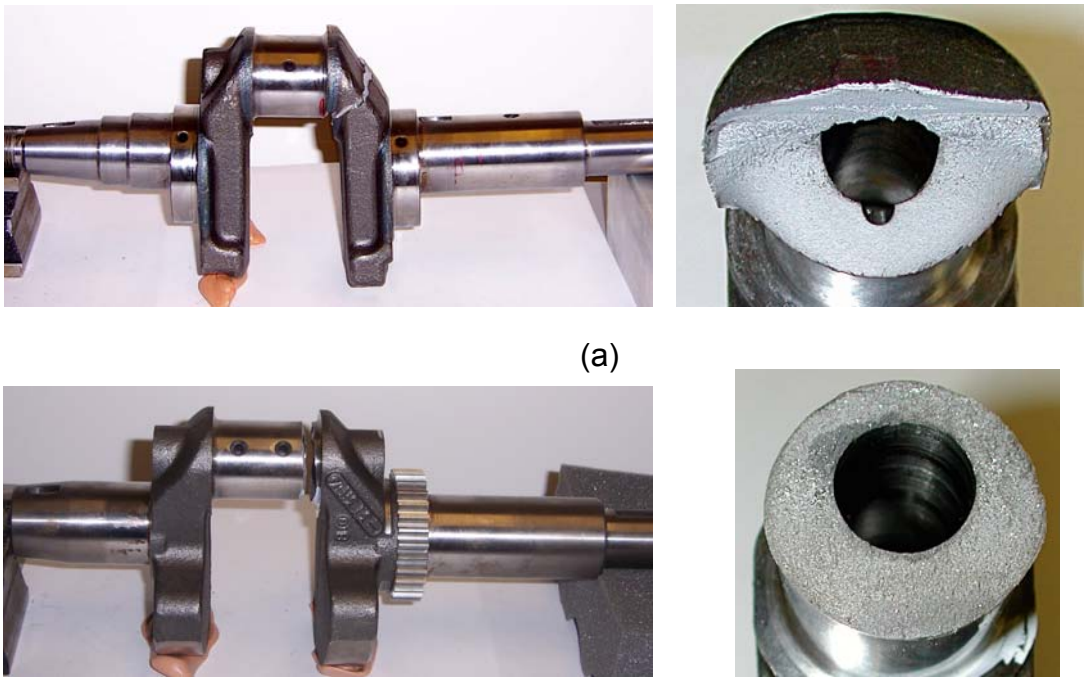

(a)

(b)

Figure 17: Typical fatigue fracture of the (a) forged steel crankshaft, and (b) of the ductile cast iron crankshaft.

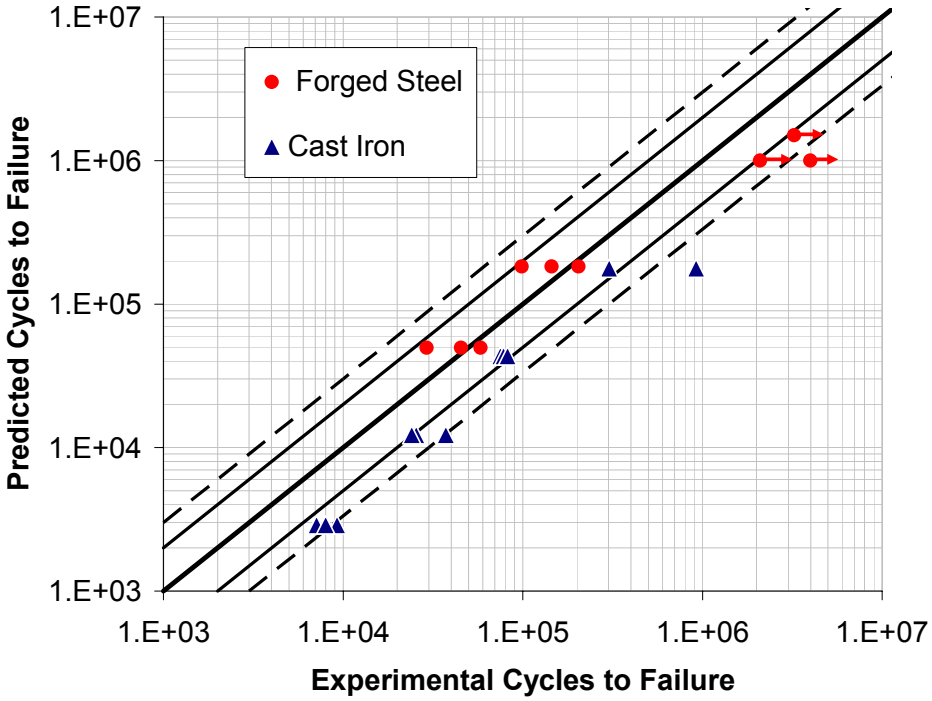

Figure 18: Predicted cycles to failure versus experimental cycles to failure for the two crankshafts using the S-N approach.

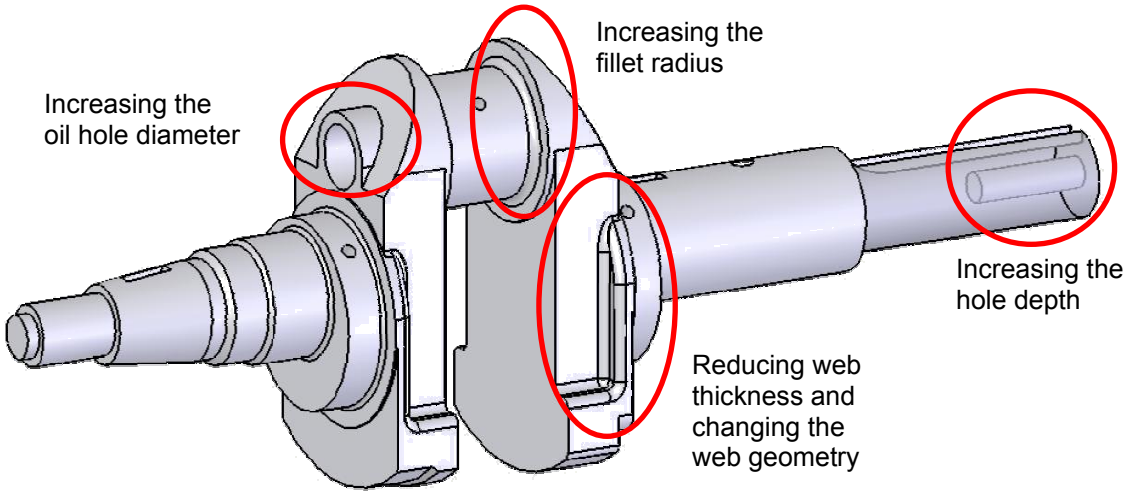

(a)

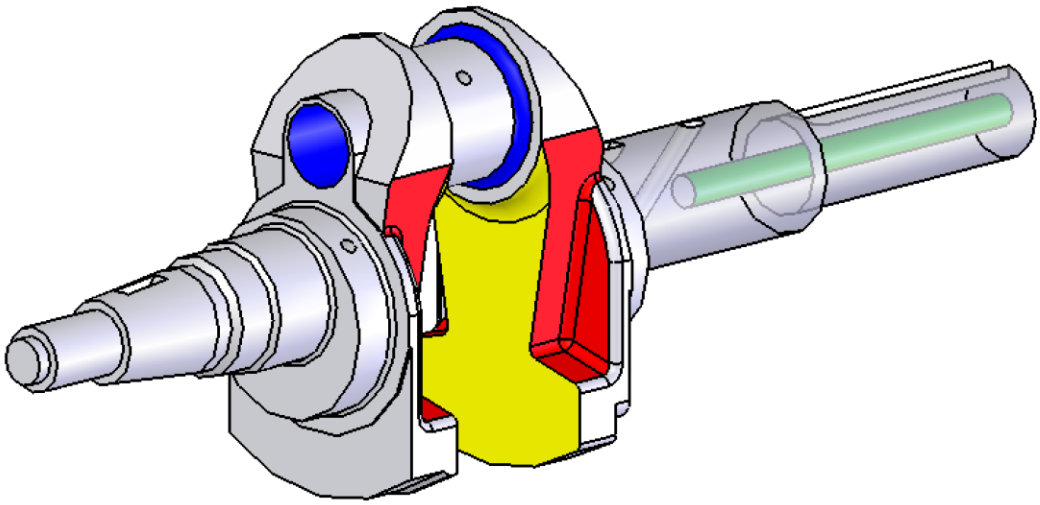

(b)

Figure 19: Original crankshaft showing locations where optimization was applied (a), and final optimized geometry (b).